JOURNAL OF ROCK MECHANICS

VOL. 9, NO. 4, PP. 73-91.

https://doi.org/10.22034/IRSRM.2026.739361.1083

# Evaluation of the effect of temperature and number of heating-cooling cycles on the damage of rock salt

**Ali Kalantari Dehaghi[1], Ebrahim Farrokh[1*], Hamed Molladavoodi[1]**
**1. Department of Mining Engineering, Amirkabir University of Technology, Tehran, Iran.**

**Received: 22 January 2026 Accepted: 20 March 2026**
**(*Corresponding author: e.farrokh@aut.ac.ir)**

**Keywords**

**Rock salt**
**Thermal cycles**
**Temperature**
**Uniaxial compressive strength**
**Damage**

**Abstract**

Rock salt is recognized as one of the most important host rocks for underground storage of natural gas, hydrogen, and nuclear waste disposal due to its characteristics, such as very low permeability, low porosity, viscoplastic behaviour, self-healing capability, and suitable stability. However, during the operation of salt caverns, repeated fluid injection and withdrawal processes cause alternating temperature changes and thermal cycles in the rock mass. These cycles, through repeated thermal expansion and contraction, induce internal stresses, microcrack growth, and structural changes in the rock salt, which can affect the mechanical and physical properties of the rock and, in the long term, reduce the stability and safety of underground reservoirs. Therefore, understanding the behaviour of rock salt under different thermal conditions is of particular importance. The main objective of this study is to investigate the simultaneous effect of temperature and heating–cooling cycles on the mechanical behaviour and the extent of damage in rock salt. To achieve this goal, cubic rock salt samples were prepared and subjected to three temperature levels: ambient temperature (25°C), 50°C, and 80°C, as well as to 1, 5, and 10 thermal cycles. The results showed that increasing the temperature and the number of thermal cycles causes noticeable changes in the internal structure of rock salt and reduces its mechanical properties, including uniaxial compressive strength and elastic modulus.

## I. INTRODUCTION

Rapid heating–cooling cycles (weekly, daily, or even shorter) are strongly observed in natural gas and hydrogen storage sites. These operational conditions must be carefully investigated because rapid pressure reduction during withdrawal causes rapid cooling of the gas. Due to limited heat transfer with the surrounding rock, thermal contraction occurs in the rock, leading to tensile stresses. Given the low tensile strength of rock salt (approximately 1–2 MPa), these stresses must be controlled to maintain rock mass integrity [1]. The permissible pressure and temperature limits for safe underground natural gas storage in salt caverns are 15–30 MPa and 80°C, respectively [2]. Salt cavern gas storage is typically buried at depths of 600–800 m, where the geothermal gradient of approximately 3°C per 100 m yields in-situ rock temperatures of 38–44°C before operational loading [3]. The upper bound of 80°C corresponds to the maximum permissible temperature for safe underground natural gas storage and represents a critical scenario when injection-induced thermal loading is superimposed on the geothermal baseline. The intermediate temperature of 50°C was included to capture the transitional damage behavior between ambient (25°C) and operational upper-limit conditions.

Tests for assessing damage in rock samples are divided into two categories: destructive and non-destructive. In this study, damage was evaluated through destructive uniaxial compressive strength (UCS) testing. Compressive strength is the maximum stress that an intact rock sample can withstand before failure [4]. UCS testing has many applications, including tunnel construction [5], underground caverns, powerhouses, mining operations [6], rock burst assessment [7], dam construction, stability evaluation of substructures on rock, and rock slopes. Furthermore, UCS testing is critically important in evaluating storage stability and is one of the key tests in understanding the response of rock to mechanical stresses under different loading conditions [8, 9]. It is also one of the key parameters in geomechanical classification systems for rock masses such as RMR and Barton's Q system [10, 11]. Cyclic thermal loading is a critical consideration across a range of geomaterials and geotechnical applications, from underground gas storage in rock salt to frost-susceptible soils in cold-region infrastructure [12].

Numerous studies have been conducted on the mechanical properties and long-term behavior of rock salt, but research specifically investigating the effect of temperature on these properties is limited. In previous studies, three different laboratory approaches have been observed:

- Heating samples to specific temperatures using special thermal equipment attached to the testing apparatus
- Heating samples in an oven and testing immediately after removal
- Using samples that were heated and then cooled to room temperature
- Using samples that were heated and then cooled in water

Zhou et al. [13] experimentally investigated the effect of two types of thermal processes: natural heating and cooling, and heating with water cooling cycles at temperatures ranging from 200 to 1000°C. They showed that after each cycle, mechanical properties such as compressive strength, Young's modulus, peak strain, and deformation modulus changed. Under natural cooling, mechanical properties showed no significant change up to approximately 400°C, but above the threshold temperature of 600°C, a significant reduction in strength and elastic modulus occurred, and the failure behavior changed from brittle to ductile. Under water cooling, a slight increase in strength and deformation modulus was observed at temperatures below 400°C, attributed to the closure of natural microcracks. However, at 600°C and above, rapid cooling caused severe thermal stresses and microcrack propagation, leading to a sharp reduction in compressive strength.

Brotóns et al. [14] investigated the effect of temperature and cooling method on the physico-mechanical properties of San Julián calcarenite, a porous rock. The aim was to study changes in UCS, elastic modulus, Poisson's ratio, porosity, damping, ultrasonic wave velocity, and rock durability after heating in the temperature range of 100–600°C, as well as the effect of two cooling methods (air cooling and water cooling). Results showed that the elastic modulus decreased by 75% (air cooling) and 78% (water cooling) at 600°C. UCS decreased by 34% (air cooling) and 50% (water cooling).

Gautam et al. [15] experimentally investigated the effect of repeated heating–cooling cycles on the physical and mechanical properties of four different granite types. At 250°C after 9 thermal cycles, the elastic modulus decreased by 59.64%, 49.1%, 73.99%, and 54.57% for pink, red, golden, and white granite, respectively. Fracture strain increased by 373.47%, 122.42%, 199.61%, and 90.27%, respectively.

Isaka et al. [16] investigated the behavior of Harcourt granite in the temperature range of 25–1000°C under two cooling methods: rapid cooling (water immersion) and slow cooling (in-oven cooling). UCS and Young's modulus increased slightly up to approximately 100°C (due to closure of initial cracks). Beyond this temperature, both parameters decreased sharply. At 600–1000°C, strength reduction was severe, with up to more than 80% reduction in maximum strength. Rapid cooling caused more degradation than slow cooling due to thermal shock and sudden microcracking.

Guo et al. [17] experimentally investigated the effect of heating–cooling cycles on the physical and mechanical properties of rock salt. Cylindrical rock salt samples were subjected to temperatures of 40–60°C and thermal cycles of 5, 10, 20, and 40. Results showed that after 40 thermal cycles, UCS and elastic modulus decreased by 23.8% and 27.4%, respectively.

Li et al. [18] investigated the mechanical behavior of three types of rock salt under different temperature conditions. The compressive strength of the three rock salt types at 53°C was approximately 65, 77, and 82 MPa, respectively, which decreased to 46, 52, and 55 MPa at 65°C. This represents an average reduction of 30–35% in compressive strength with increasing temperature.

Liu et al. [19] experimentally investigated the fatigue and damage of rock salt under different cycles. Results showed that increasing the number of cycles or increasing the maximum temperature reduced compressive strength and elastic modulus while increasing rock ductility. According to their findings, this softening effect is significantly intensified when the maximum temperature increases from 100°C to 120°C.

Studies on the effect of temperature and number of thermal cycles show that increasing temperature and cycle counts does not always reduce compressive strength, elastic modulus, and other mechanical and physical properties of rocks. In some cases, the trend is completely opposite up to a certain temperature threshold. Therefore, this study investigates the effect of temperature and different cycles specifically on rock salt. Thus, investigating the effect of temperature on the mechanical properties of rock salt is essential for accurate long-term stability assessment of natural gas storage in salt caverns (SCGS) [20].

In this study, the effect of three different temperatures (25°C, 50°C, and 80°C) combined with 1, 5, and 10 thermal cycles was investigated on cubic rock salt samples.

## II. METHODOLOGY

According to the experimental design Samples were heated from ambient temperature (25 ± 2°C) to the target temperature at an oven heating rate of approximately 3 °C/min, after reaching the target temperature, samples were held at that temperature for 12 hours. This dwell time ensures that the sample temperature becomes completely uniform, full thermal expansion occurs, internal thermal stresses have time to develop, and microcracks are generated at a small scale. After completing the 12-hour heating period, the oven was turned off, and the samples were naturally cooled (air cooling in the laboratory environment) at average rate of 3 °C/min. The cooling duration was also 12 hours in the laboratory at a temperature of 25 ± 2°C.

During this stage, the samples cooled from 50°C or 80°C to room temperature, and thermal contraction occurred. The combination of expansion (during the heating stage) and contraction (during the cooling stage) is the main cause of microcrack generation. The steps of this process are shown in Figure 1.

Uniaxial compressive strength tests were conducted in accordance with ASTM D7012 [21]. To ensure uniform stress transfer across the specimen surfaces, the top and bottom faces of all cubic specimens were coated with a thin, uniform layer of soft paraffin wax was maintained below 1 mm to ensure negligible prior to testing. This capping layer reduced surface irregularities and promoted uniform load distribution across the full contact area. The paraffin layer thickness influence on the test results, consistent with the recommendations of ASTM D7012 – Method C for the use of capping materials on non-standard specimen geometries.

Tests were performed under displacement-controlled loading at a rate of 0.6 mm/min. Load and displacement data were recorded at a sampling frequency of 2 Hz throughout each test. The load cell had a maximum capacity of 2000 kN with a measurement accuracy of 0.5% of full scale, corresponding to a force resolution of 0.01 kN. Axial deformation was measured using LVDTs. All testing parameters were identical across all specimens, including the control group, ensuring direct comparability of results.

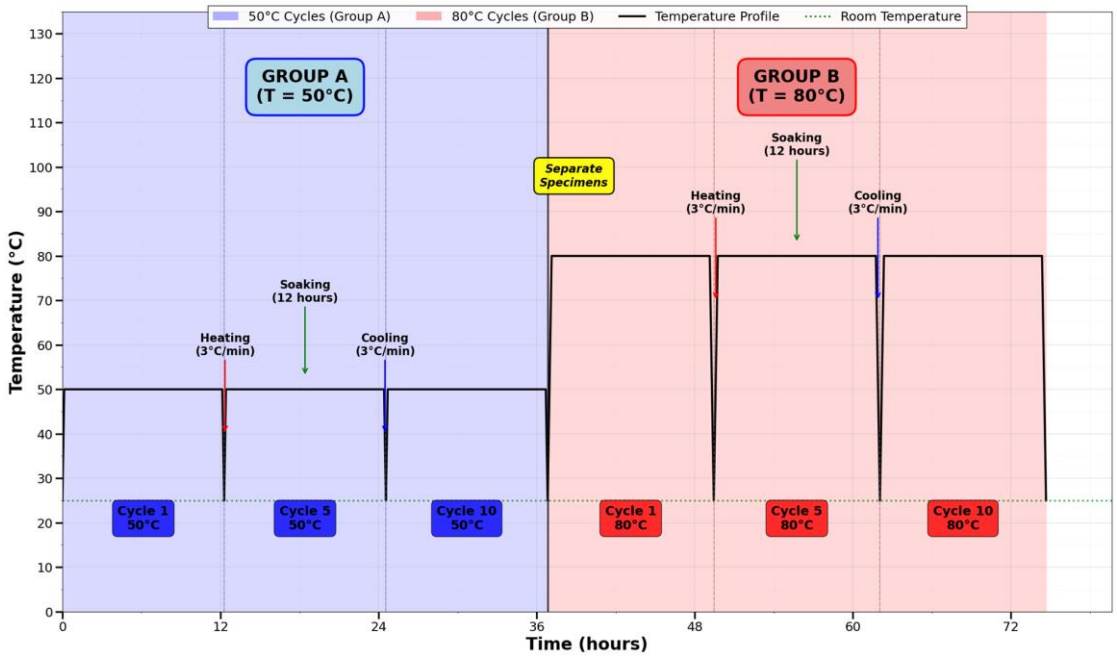


Fig. 1. Schematic diagram of the heating-cooling cycle process

## A. *Sample specifications*

Rock salt (halite) with the chemical formula NaCl is a crystalline and isometric material that exhibits completely brittle behaviour at low temperatures and completely ductile behaviour at high temperatures. The major characteristics of rock salt that are important in this research are:

- Anisotropy of wave velocity due to the orientation of cleavage planes
- High sensitivity to microcracks
- Change in moduli with increasing temperature
- Decrease in strength with an increasing number of heating-cooling cycles

## B. *Sample preparation*

All samples were taken from a relatively homogeneous block of rock salt to minimize side effects caused by textural variations. Using a diamond rock cutting machine, the samples were cut with an accuracy of 1 mm. For performing the ultrasonic test, completely smooth surfaces were required. Therefore, the surfaces were polished using sandpaper grits 200, 400, 800, and 1200. For sample preparation according to the number of cycles, 2 cubic samples with dimensions of 8×8×8 cm were prepared for each cycle. Additionally, 3 samples were prepared as control samples to record the baseline values of uniaxial compressive strength, so that the results obtained at different temperatures and cycles could be compared with these reference values. The average of the results obtained from these replicates was recorded as the baseline values for assessing the extent of damage in the rock at

temperatures of 50°C and 80°C. An image of the cubic rock salt sample after cutting and coding, ready for heating at 50°C in cycles 1, 5, and 10, is shown in Figure 2. Figure 3 also shows the samples after being placed in the oven and before heating. Cubic specimens were used in this study rather than the standard cylindrical geometry, primarily because the flat parallel surfaces of cubes facilitate consistent ultrasonic wave transmission measurements and simplify sample preparation by eliminating coring. It is acknowledged that cubic specimens introduce end friction effects that are somewhat different from those in cylinders, and that the height-to-width ratio of 1.0 used here is lower than the standard 2.0–2.5 for cylinders, which tends to produce slightly higher apparent UCS values due to end confinement effects. However, since all specimens in this study share identical geometry, these systematic effects cancel in the relative comparisons and in the damage variable D, which is defined as a normalized ratio. The use of cubic specimens for rock salt is consistent with the approach adopted by Maadikhah et al [22]. Investigating the scale effect on the results of this search show that increasing specimen size generally increases the probability of containing critical pre-existing flaws and a greater total population of microcracks and fractures. This effect would be expected to produce somewhat lower absolute UCS values and an earlier onset of failure in larger rock salt specimens compared with the 80 mm cubes used in this study. However, this effect is tempered by several factors specific to the present study. First, rock salt is exceptionally homogeneous and isotropic at the grain scale compared with most rock types, lacking the large-scale structural discontinuities (joints, bedding, mineral banding) that drive pronounced size effects in heterogeneous lithologies; consequently, the size sensitivity of intact rock salt strength is generally reported to be weaker than in jointed or heterogeneous rock masses. Second, and most critically for the conclusions of this study, the damage variable D is defined as a normalized ratio between the thermally cycled and intact specimen properties. Because any systematic size-related reduction in absolute strength would be expected to act similarly on both the numerator and denominator of this ratio, the size-dependent bias is expected to substantially cancel in the normalized damage metric, even though the absolute UCS and elastic modulus values reported here may differ moderately from values obtained using larger specimens.

### *C. Classification of test specimens*

After preparation, the samples were divided into three groups: C, D, and E. Group C consisted of 3 samples for recording baseline values for uniaxial compressive strength. The physical and mechanical properties of the control group is shown in Table 6. Group D consisted of a total of 6 samples at 50°C, with 2 samples selected for each of the 1, 5, and 10 thermal cycles. Group E consisted of 6 samples at 80°C, with 2 samples used for each of the 1, 5, and 10 thermal cycles. A total of 15 samples were tested. The sample grouping is shown in Table 1.

TABLE I. CLASSIFICATION OF THE SPECIMENS

| Group name | Group code | T | Number of cycles | Number of specimens |
|---|---|---|---|---|
| C | T-25-C0 | 25 | 0 | 3 |
| D | T-50-C01 | 50 | 1 | 2 |
| D | T-50-C05 | 50 | 5 | 2 |
| D | T-50-C10 | 50 | 10 | 2 |
| E | T-80-C01 | 80 | 1 | 2 |
| E | T-80-C05 | 80 | 5 | 2 |
| E | T-80-C10 | 80 | 10 | 2 |
| Total | - | - | - | 15 |

The behaviour of rock salt under thermal cycling is a complex phenomenon that is a function of two key parameters: temperature and number of cycles. As discussed earlier, increasing each of these parameters individually leads to weakening of the rock structure and reduction of its mechanical properties. However, in real applications, these two factors often act synergistically; that is, their combined effect is greater than the sum of their individual effects. To quantitatively evaluate this degradation, two key parameters are examined in studies [13].

- Reduction in uniaxial compressive strength: This parameter represents the maximum stress that the rock sample can withstand before failure. A decrease in compressive strength directly indicates the overall weakening of the rock structure.
- Reduction in elastic modulus: The elastic modulus is a measure of the stiffness and rigidity of the material. Its decrease indicates an increase in rock flexibility and, more importantly, an increase in crack growth and weakening of intergranular bonds


Fig. 2. Cubic rock salt specimens


Fig. 3. Cubic rock salt specimens ready for heating to 50°C.

*D. Damage variable*

*1)* Uniaxial compressive strength

The changes in uniaxial compressive strength due to the simultaneous effect of temperature and number of thermal cycles, relative to the initial compressive strength of the rock, were investigated as one of the main parameters for evaluating the extent of damage induced in the rock in this study. In general, the amount of damage caused by temperature and heating–cooling cycles is obtained from Equation 1.

$$D_{(T,n)} = 1 - \frac{UCS_{(T,n)}}{UCS_0} \quad (1)$$

where $D_{(T,n)}$ is the damage induced at temperature T and after n cycles, $UCS_{(T,n)}$ is the compressive strength value after n thermal cycles at temperature T, and $UCS_0$ represents the initial compressive strength of the rock at 25°C [13].

*2) Elastic modulus*

The elastic modulus, as another strength parameter of the rock, reacts to increasing temperature and increasing number of cycles and follows a decreasing trend. The extent of damage induced in the rock can also be defined based on the reduction in elastic modulus at different temperatures and cycle numbers according to Equation 2:

$$D_{(T,n)} = 1 - \frac{E_{(T,n)}}{E_0} \quad (2)$$

where $D_{(T,n)}$ is the damage induced based on the reduction in elastic modulus, $E_{(T,n)}$ is the elastic modulus value after n thermal cycles at temperature T, and $E_0$ represents the initial elastic modulus of the rock at 25°C [13].

## III. RESULTS

After sample preparation, the thermal cycles were applied according to the procedure described in the research methodology. Then, after each cycle, all samples were tested using a uniaxial loading device with a static and identical loading rate. Figure 4 shows the uniaxial compressive strength test before and after 10 thermal cycles at 50°C. A summary of the results is reported in Table 2.

To increase the accuracy of the results obtained from the uniaxial test, each experiment at the target temperature and cycle was performed on two samples, and the final stress-strain curve was plotted by taking the average of these values. Figure 5 shows the stress-strain curves obtained at temperatures of 25, 50, and 80°C and at cycles 1, 5, and 10. With increasing temperature and number of cycles, the maximum strength of rock salt decreases significantly, reaching from its highest value at 25°C with no thermal cycle to its lowest value at 80°C after 10 heating–cooling stages. The compressive strength after 10 thermal cycles at 50°C decreases by approximately 25% compared to the control sample, and this reduction reaches approximately 60% at 80°C after 10 thermal cycles. The strength reduction between 1 and 5 cycles is approximately 21.6% of the initial compressive strength at 80°C versus only 3% at 50°C. The reduction between 5 and 10 cycles is approximately 28.8% at 80°C and 17% at 50°C.

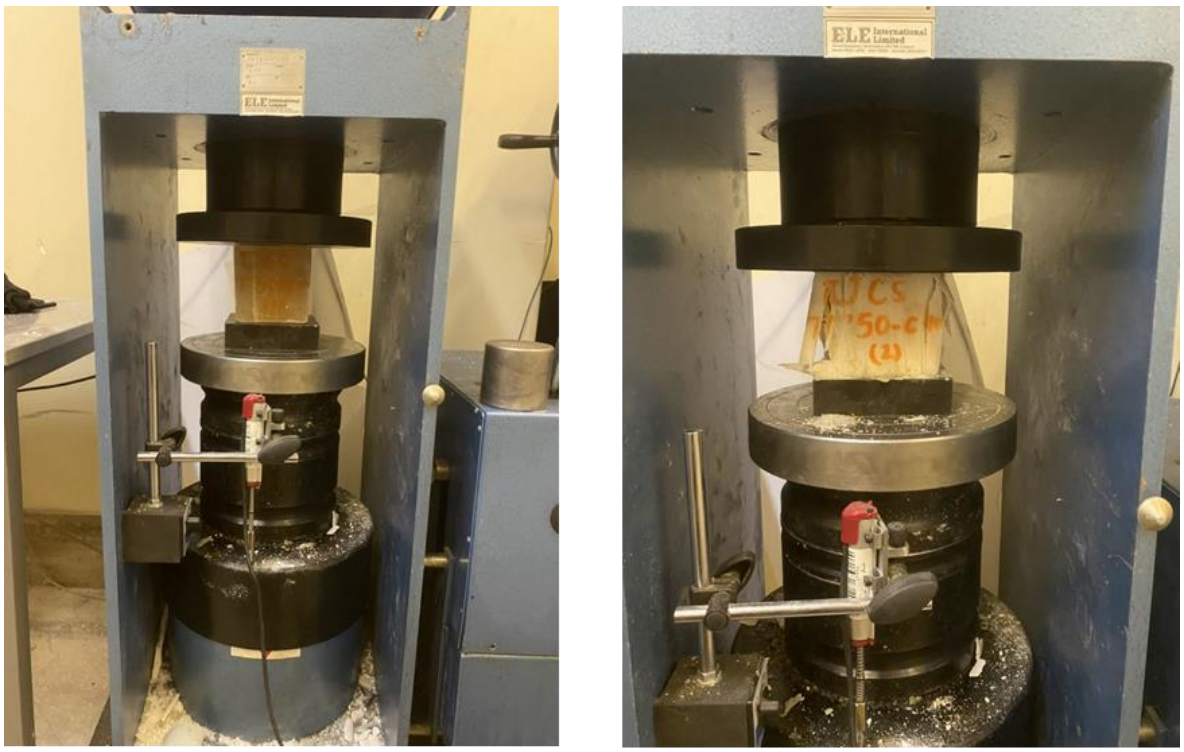


Fig. 4. Uniaxial test after ten thermal cycles at 50°C: (a) before loading (b) after loading

Throughout this paper, peak strain is defined as the axial strain corresponding to the maximum stress (UCS) on the stress-strain curve. The peak strain in the control sample at 25°C has the highest value. At 50°C, the peak strain increases consistently but modestly with cycle number, with the 50°C specimens clustering tightly between 2.41% and 2.56% a narrow band indicating that peak strain at this temperature is relatively insensitive to cycle number once the first cycle has been completed. At 80°C, the peak strain increases more rapidly across all three cycle counts, with a single cycle at 80°C producing more peak strain increase than ten complete cycles at 50°C. Detailed peak strain values are provided in Table 2.

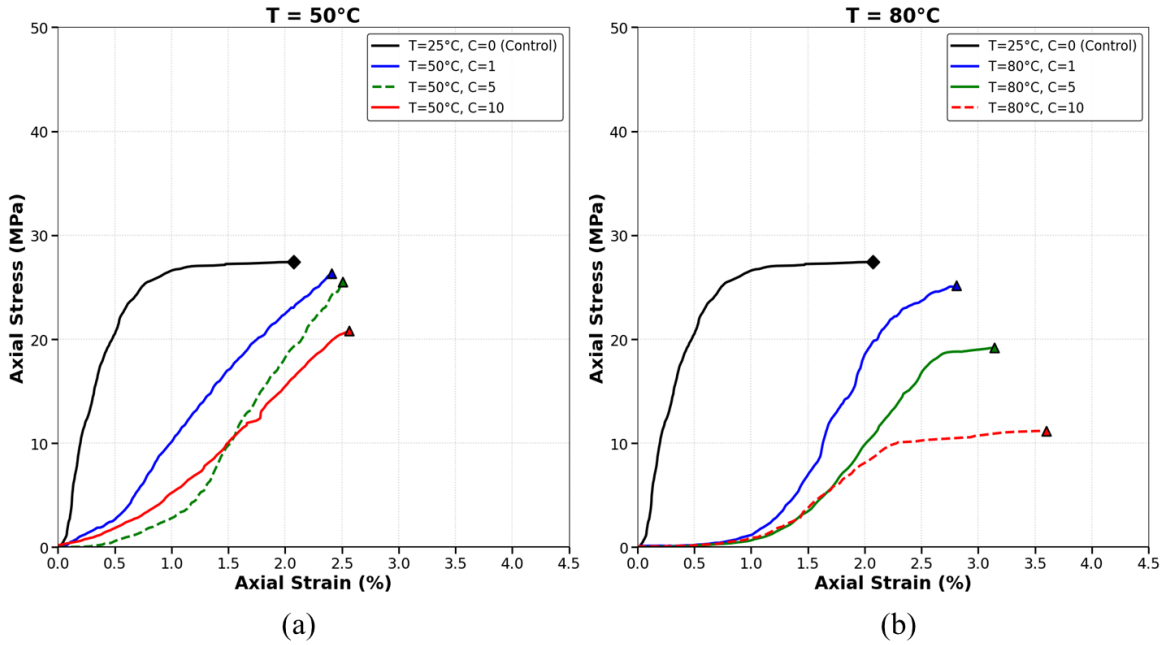


Fig. 5. Stress-strain curve in different cycles: (a) at T=50°C (b) at T=80°C

TABLE II. PEAK STRAIN RESULTS UNDER DIFFERENT THERMAL CONDITIONS

| T(°C) | Cycle | Peak Strain (%) | Standard deviation | Increase vs control (%) | Increase from previous cycle (pp) |
|---|---|---|---|---|---|
| **25** | 0 | 2.07 | 0.045 | - | - |
| **50** | 1 | 2.41 | 0.07 | +16.3 | +0.34 |
| **50** | 5 | 2.5 | 0.10 | +20.8 | +0.09 |
| **50** | 10 | 2.56 | 0.12 | +23.6 | +0.06 |
| **80** | 1 | 2.8 | 0.18 | +35.3 | +0.73 |
| **80** | 5 | 3.14 | 0.13 | +51.6 | +034 |
| **80** | 10 | 3.60 | 0.17 | +73.5 | +0.46 |

pp = Percentage points

The stress-strain curves at different temperatures and thermal cycles, along with the boundary points of crack closure, damage onset, and uniaxial compressive strength are shown in Figure 7. The threshold points are CC (crack closure), CD (crack damage), and UCS (uniaxial compressive strength). The crack closure threshold (CC, Point A) was identified as the inflection point at which the initial concave-upward nonlinearity of the axial stress-strain curve transitions to approximately linear behavior. The crack damage threshold (CD, Point B) was identified as the point of departure from linearity prior to peak stress, where the curve begins to exhibit upward convexity again, indicating the onset of unstable microcrack propagation. Both thresholds were identified independently for each specimen and the average value was adopted. To provide an objective and quantitative basis for crack damage threshold detection a volumetric strain reconstruction method was applied to the existing dataset. This approach derives volumetric strain entirely from the measured axial stress-strain data and the elastic properties of the specimen, without requiring lateral strain gauges or acoustic emission monitoring. The dynamic Poisson's ratio was calculated from the compressional (Vp) and shear (Vs) wave velocities measured on each specimen prior to thermal cycling and after each cycle in different temperatures, using the standard elastic wave relation [23]. For rock salt specifically, the relationship between static and dynamic Poisson's ratio has been documented in the literature [24]. In this study the static poisson's ratio is calculated from Equation 4.

$$\upsilon_{dyn} = \frac{V_p^{\,2} - 2V_s^{\,2}}{2(V_p^{\,2} - V_s^{\,2})} \quad (3)$$

$$\upsilon_{static} = 0.64.\upsilon_{dynamic} + 0.065 \quad (4)$$

For thermally cycled specimens, $\upsilon_{dyn}$ was recalculated from ultrasonic measurements taken after each thermal cycling condition using Equation 3, and $\upsilon_{stat}$ was then estimated using Equation 4. This assumption is considered valid given that the conversion factor reflects an intrinsic material characteristic of the halite crystal structure rather than a thermally sensitive parameter. The volumetric strain in uniaxial test is obtained from Equation 5.

$$\varepsilon_{vol} = \varepsilon_{ax}(1 - 2\upsilon_{sta}) \quad (5)$$

By calculating volumetric strain for each point, the volumetric strain curve against axial strain is plotted. The reconstructed volumetric strain versus axial strain curve exhibits a characteristic shape that directly reveals the damage threshold points, as illustrated schematically in Figure 6. During the crack closure phase (origin to CC): The curve is nonlinear because pre-existing cracks are closing, making the apparent lateral expansion smaller than that predicted by υsta. Volumetric strain is positive and decreasing (net compression). During the elastic phase (CC to CD): The relationship between $\varepsilon_{vol}$ and $\varepsilon_{ax}$ is approximately linear. At the crack damage threshold (CD, Point B&F): This is defined as the inflexion point of the volumetric strain curve, where:

$$\frac{d\varepsilon_{vol}}{\varepsilon_{ax}} = 0 \quad (6)$$

At this point, the rate of volumetric dilation due to microcrack opening exactly equals the rate of elastic compression due to continued axial loading. Beyond this point, crack dilation dominates and volumetric strain begins to increase back toward zero. At peak stress (UCS): The volumetric strain returns to approximately zero, meaning the specimen has dilated back to approximately its original volume, as crack-induced expansion has offset the elastic compression accumulated during loading [25]. At 50°C, the reconstructed volumetric strain curve shows continuous decrease (net compression) from the start of loading to peak stress, with no inflection point. This would confirm that the specimen fails before crack dilation overcomes elastic compression, consistent with more brittle failure behavior at this temperature. In this case, $\varepsilon_{vol}$ at peak stress remains positive, meaning the specimen is still in net compression at failure. All threshold values with standard deviations are reported in Table 3.

The control specimen achieves a UCS of 27.68 ± 0.65 MPa, representing the intact material's maximum load-bearing capacity. The crack closure zone ends at a strain of just 0.08 ± 0.003% and a stress of only 1.44 ± 0.06 MPa. The crack damage threshold (Point B) occurs at 0.73 ± 0.02% strain and 24.96 ± 0.70 MPa, representing 90.1% of the peak UCS.

At 50°C, the degradation is initially modest, with UCS reductions of 4.8%, 7.9%, and 24.8% after 1, 5, and 10 cycles respectively. The crack closure strain grows progressively with cycle number at 50°C. One of the most significant findings is that the crack damage threshold (Point B) is entirely absent in all three 50°C specimens, the stress-strain curve transitions directly from the elastic region into the peak strength point with no identifiable intermediate damage threshold.

At 80°C, the degradation trajectory is more severe and sets in earlier, with UCS reductions of 9.1%, 30.7%, and 59.5% after 1, 5, and 10 cycles respectively. The crack closure zone at 80°C is consistently and substantially wider than at 50°C across all cycle counts. At 80°C, a distinct crack damage threshold appears in every specimen. The consistent B/C stress ratio of roughly 66–80% across all specimens that show Point B suggests this is a material-intrinsic proportion, maintained even as the absolute stress levels collapse. The elastic zone, spanning from Point A to Point B (or to peak for 50°C specimens), represents the region of recoverable linear deformation. In the control, this zone spans 0.65% strain across a stress range of 23.52 MPa. At 50°C, the elastic stress range drops from ~18 MPa at C=1 and C=5 to 11.02 MPa at C=10, a 46.85% narrowing. At 80°C, the elastic zone is severely compressed, reaching just 7.18 MPa at C=10, less than 30.6% of the control's elastic stress range.

The changes in compressive strength and elastic modulus with increasing number of cycles and temperature are shown in Figures 8 and 9 respectively. The UCS decreases monotonically under all thermal conditions while the elastic modulus exhibits a non-monotonic response, initially increasing at low cycle counts before collapsing at higher cycle counts. All values are summarized in Table 4. The most notable observation regarding elastic modulus is that at 80°C after one cycle, the modulus surges to 2.17 ± 0.11 Gpa, the single highest value in the entire dataset, representing a 64.4% increase above the control. Similarly, at 50°C after five cycles, the modulus recovers to 1.62 ± 0.10 GPa, a 22.7% gain above the control. However, both series ultimately collapse under accumulated fatigue at ten cycles, reaching 0.80 ± 0.04 GPa at 50°C and 0.25 ± 0.01 GPa at 80°C.

The temperature-dependent behavior of elastic modulus reverses completely with increasing cycle count. After 1 cycle, higher temperature produces dramatically higher stiffness: 2.17 ± 0.11 GPa at 80°C versus 1.17 ± 0.07 GPa at 50°C, a difference of 1 GPa (85.5% higher at 80°C). After 5 cycles, this

advantage has largely eroded, with 50°C now producing a slightly stiffer material by 0.26 GPa (19.1% higher at 50°C). After 10 cycles, the reversal is complete and extreme, with 50°C being 220% stiffer than 80°C, and the ratio between the two moduli reaching 3.20.

Figure 10 shows the thermal damage variable D based on UCS under all thermal conditions. All D values are strictly positive throughout, meaning every thermal condition produces genuine net strength loss with no healing anomaly. Compressive strength degrades monotonically from the very first cycle without exception, and no combination of temperature and cycle number reverses this trend even partially. At 50°C, the acceleration of damage between five and ten cycles is particularly sharp, with that final interval alone accounting for nearly 67% of the total accumulated damage across all ten cycles. At 80°C, the damage progression is far more aggressive at every cycle count. Figure 7(b) shows the slopes of all three cycle-count lines steepening dramatically between 50°C and 80°C, with the ten-cycle series showing the steepest gradient of all.

Figure 11 shows the damage variable D based on elastic modulus. Unlike D(UCS), the elastic modulus damage variable exhibits strongly negative values at low cycle counts, indicating net stiffening rather than damage. The transition from negative to positive D occurs between five and ten cycles for both temperatures.

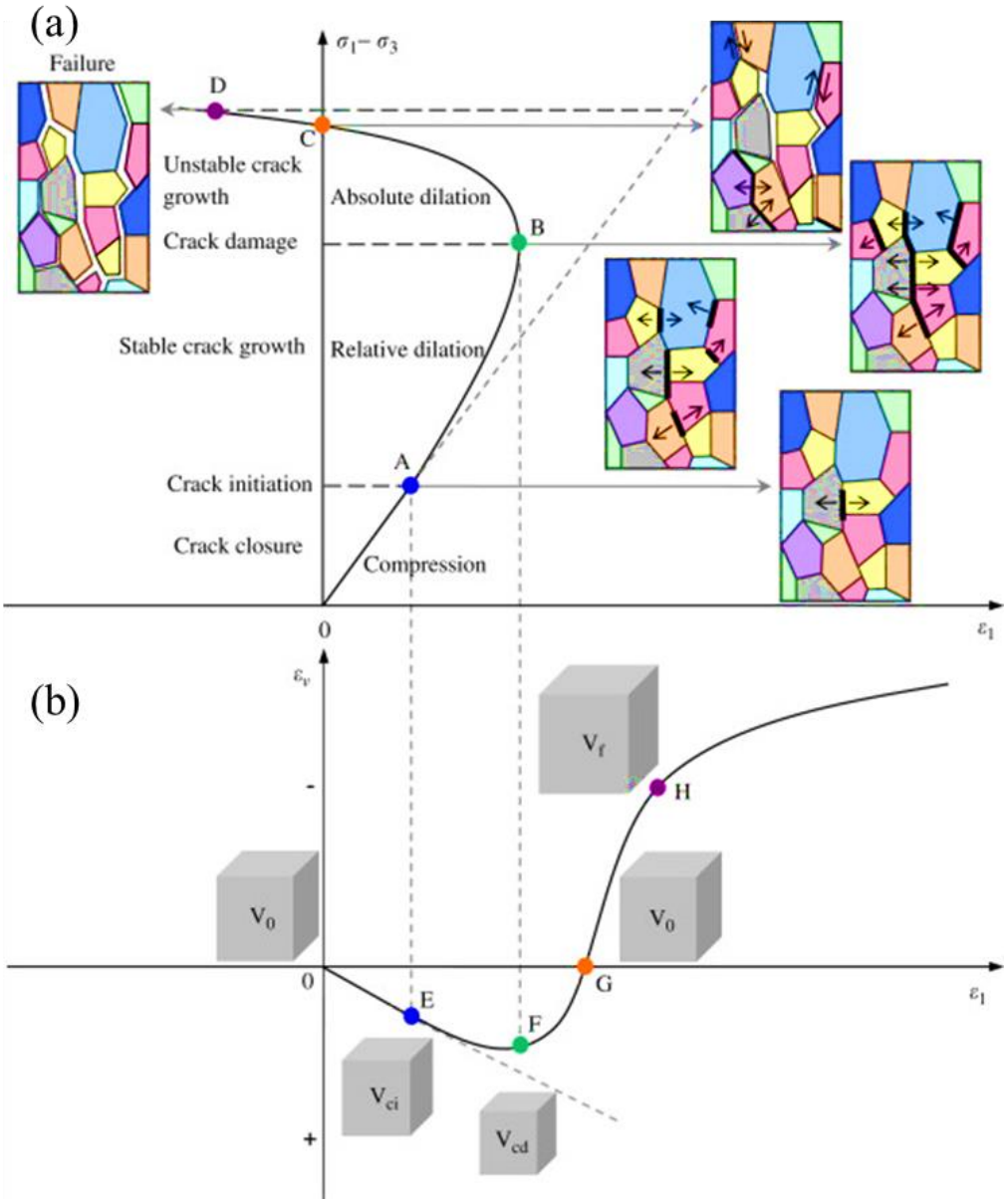


Fig. 6. (a) Deviatoric stress – axial strain and (b) volumetric strain – axial strain [25]

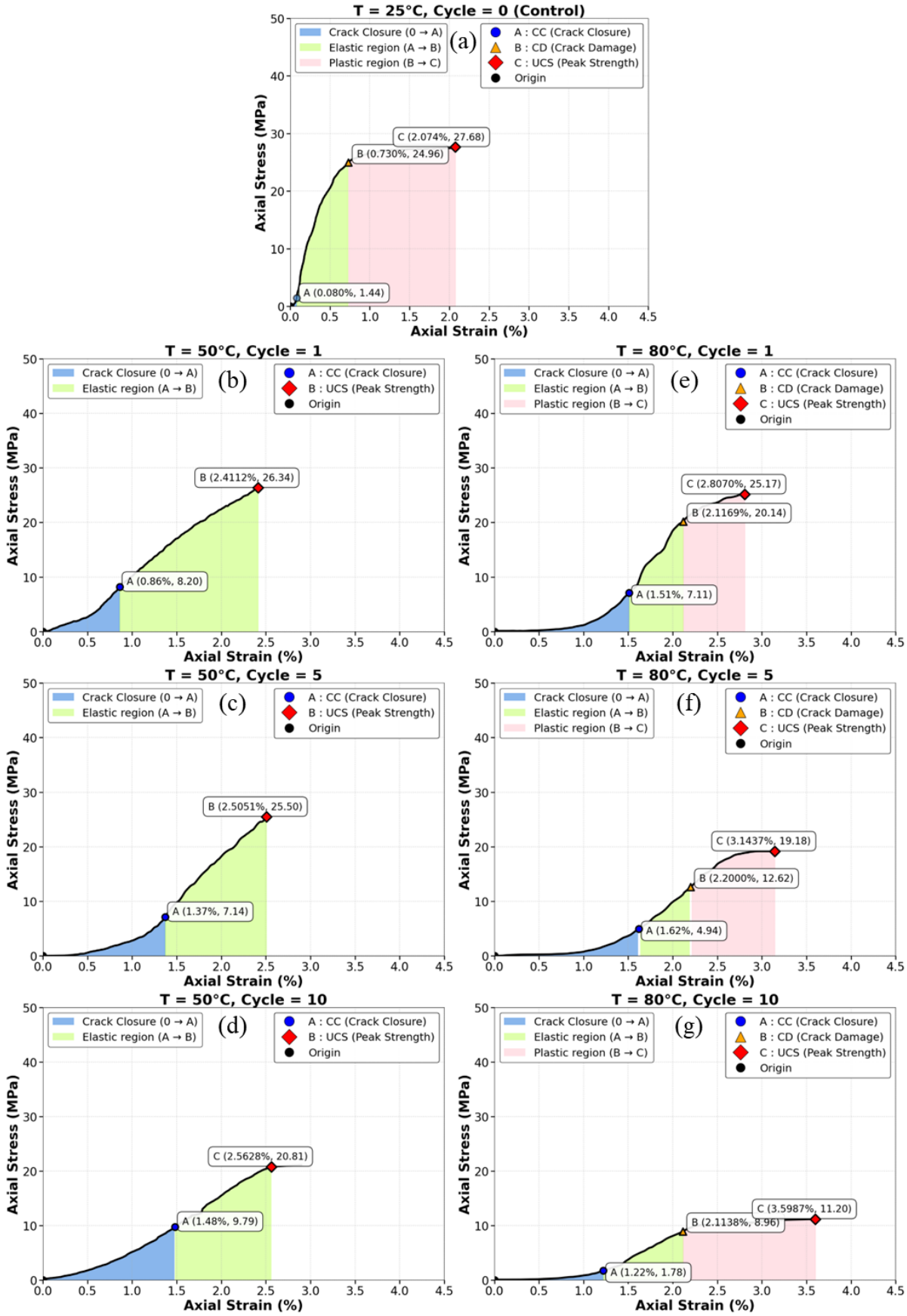


Fig. 7. Axial stress-axial strain curves: (a) control group at T=25°C (b) at 50°C and 1 thermal cycle (c) at 50°C and 5 thermal cycles (d) at 50°C and 10 thermal cycles (e) at 80°C and 1 thermal cycle (f) at 80°C and 5 thermal cycles (g) at 80°C and 10 thermal cycles

TABLE III. RESULTS OF UNIAXIAL COMPRESSIVE STRENGTH TEST WITH THRESHOLD VALUES

| T | Cycle | Threshold points | | | | | | E (GPa) |
|---|---|---|---|---|---|---|---|---|
| | | *CC* | | *CD* | | *UCS* | | |
| - | - | Stress(Mpa) | Strain(%) | Stress(Mpa) | Strain(%) | Stress(Mpa) | Strain(%) | - |
| 25 | 0 | 1.44 ± 0.06 | 0.080 ± 0.003 | 24.96 ± 0.70 | 0.73 ± 0.02 | 27.68 ± 0.65 | 2.074 ± 0.045 | 1.32 ± 0.06 |
| 50 | 1 | 8.20 ± 0.42 | 0.86 ± 0.04 | - | - | 26.34 ± 1.06 | 2.41 ± 0.07 | 1.17 ± 0.07 |
| 50 | 5 | 7.15 ± 0.49 | 1.37 ± 0.07 | - | - | 25.50 ± 1.27 | 2.50 ± 0.10 | 1.62 ± 0.10 |
| 50 | 10 | 9.80 ± 0.71 | 1.48 ± 0.06 | - | - | 20.81 ± 1.23 | 2.56 ± 0.12 | 0.803 ± 0.049 |
| 80 | 1 | 7.10 ± 0.57 | 1.51 ± 0.07 | 20.14 ± 1.06 | 2.11 ± 0.07 | 25.17 ± 1.20 | 2.80 ± 0.18 | 2.17 ± 0.11 |
| 80 | 5 | 4.95 ± 0.49 | 1.62 ± 0.10 | 12.62 ± 0.85 | 2.2 ± 0.10 | 19.18 ± 1.13 | 3.14 ± 0.13 | 1.36 ± 0.08 |
| 80 | 10 | 1.80 ± 0.28 | 1.22 ± 0.07 | 8.96 ± 0.78 | 2.11 ± 0.08 | 11.20 ± 0.99 | 3.59 ± 0.17 | 0.251 ± 0.017 |

After 1 cycle, the two temperature series are on opposite sides of zero. After 5 cycles, both series have converged toward the center and are both negative. After 10 cycles, both series are positive but at vastly different severity levels. All damage variable values are summarized in Table 5. The key finding from the combined damage analysis is the clear decoupling between D(UCS) and D(E): while D(UCS) remains strictly positive and increases monotonically at all conditions, D(E) becomes strongly negative at low cycle counts, reaching as low as −0.64 at 80°C after one cycle, before ultimately surging to severely positive values at ten cycles, with a total range of 1.45 D-units within the 80°C series alone. The separation between the two temperature series at C=1 is 0.76 D-units, converging to only 0.20 D-units at C=5, before diverging again to 0.42 D-units at C=10. The negative values of the thermal damage variable observed at low temperatures and early cycle numbers (e.g., −0.644 at 80°C, 1 cycle) is consistent with the established rock mechanics literature. Zhou et al. (2023) reported analogous negative damage variables subjected to heating-water cooling cycles at 200°C, attributing them to closure of natural cracks and mitigation of uneven thermal stress, an interpretation made without microstructural imaging support [13]. Similarly, Martin-Clave et al. (2021), documented non-monotonic elastic parameter evolution in rock salt, linking increases in elastic recovery capacity to internal microstructural reorganization [26]. Non-monotonic stiffness recovery in rock salt has been documented experimentally: Zhao et al. reported elastic modulus increases of up to 100.5%, supporting the physical plausibility of the strongly negative damage values observed in the present study [27]. The present findings in rock salt, where a threshold of approximately 5 cycles governs the transition from elastic modulus increase to decrease, mirror the temperature-controlled threshold behavior documented by Zhou et al. (2023), suggesting a general mechanism of competing damage and healing processes during thermal cycling of crystalline rocks.

## IV. DISCUSSIONS

The main inherent characteristic of rock salt behavior is its strain-hardening behavior. Rock salt has a high load-bearing capacity, so it typically experiences significant strain and deformation until the failure point. Most hard rocks, which are characterized by brittleness, exhibit under uniaxial testing a crack closure phase, elastic behavior, stable crack growth, and unstable crack growth until failure. However, for rock salt, the crack closure point and the failure point are not completely clear. Therefore, the deformation of salt from the start of loading to the end consists of 4 stages: Stage I: elastic contraction; Stage II: transition from brittle to ductile behavior with the formation of first cracks; Stage III: brittle and ductile behavior with the onset of damage; and finally, Stage IV: relates to the strain-hardening behavior of rock salt after failure [28]. The behavior of the rock at 50°C is mostly elastic, whereas with increasing temperature to 80°C, the rock behavior becomes more elastoplastic with creep characteristics, and this behavior becomes more pronounced with increasing number of cycles. These results are consistent with the findings of Guo et al. [17]. Therefore, increasing temperature and increasing number of thermal cycles cause the behavior of rock salt to change from brittle to ductile and flexible. The progressively diminishing rate of peak strain increase at 50°C suggests that the peak strain at 50°C is approaching a saturation level somewhere around 2.55 to 2.60%. The ductilization effect at this temperature appears to be decelerating, not accelerating, meaning that additional cycles beyond ten at 50°C would likely produce minimal further increase in peak strain. The bulk of the total ductilization effect at 50°C occurs in the very first cycle, with subsequent cycles adding progressively smaller increments. At 80°C, the rate of peak strain increase is actually accelerating rather than decelerating as cycles accumulate. This is the

opposite of the saturating behavior seen at 50°C and signals that the damage mechanism at 80°C has not reached any upper limit by ten cycles. The rock is still becoming meaningfully more deformable with each additional cycle, and the trajectory suggests that further cycling would continue to push the peak strain higher. A single cycle at 80°C produces more peak strain increase than ten complete cycles at 50°C, immediately establishing that 80°C operates in a qualitatively different deformation regime.

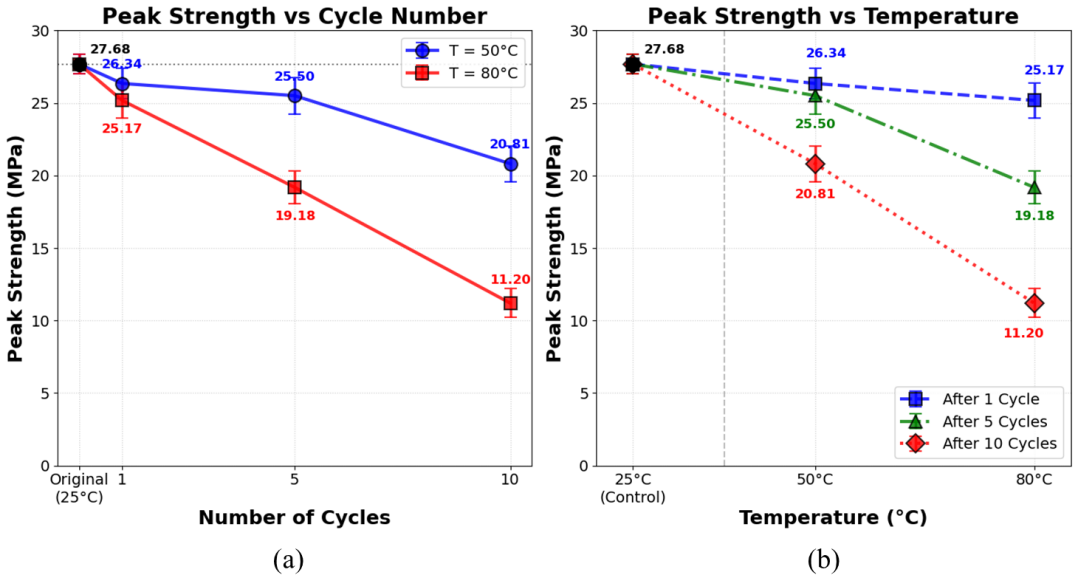


Fig. 8. Changes in compressive strength of samples: (a) with increasing number of cycles (b) with increasing temperature

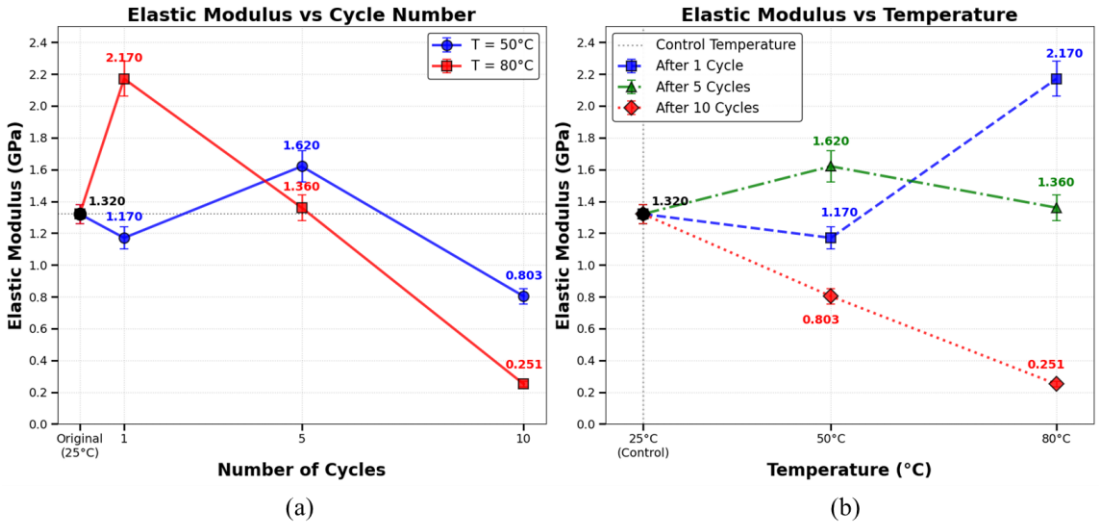


Fig. 9. Changes in elastic modulus of samples: (a) with increasing number of cycles (b) with increasing temperature

TABLE IV. UCS AND ELASTIC MODULUS RESULTS UNDER ALL THERMAL CONDITIONS

| T (°C) | Cycle | UCS (MPa) | UCS change (%) | E (GPa) | E change vs control (%) |
|---|---|---|---|---|---|
| 25 | 0 | 27.68 ± 0.03 | — | 1.32 ± 0.06 | — |
| 50 | 1 | 26.34 ± 1.06 | −4.8 | 1.17 ± 0.07 | −11.4 |
| 50 | 5 | 25.50 ± 1.27 | −7.9 | 1.62 ± 0.10 | +22.7 |
| 50 | 10 | 20.81 ± 1.23 | −24.8 | 0.80 ± 0.04 | −39.2 |
| 80 | 1 | 25.17 ± 1.20 | −9.1 | 2.17 ± 0.11 | +64.4 |
| 80 | 5 | 19.18 ± 1.13 | −30.7 | 1.36 ± 0.08 | +3.0 |
| 80 | 10 | 11.20 ± 0.99 | −59.5 | 0.25 ± 0.01 | −81.0 |

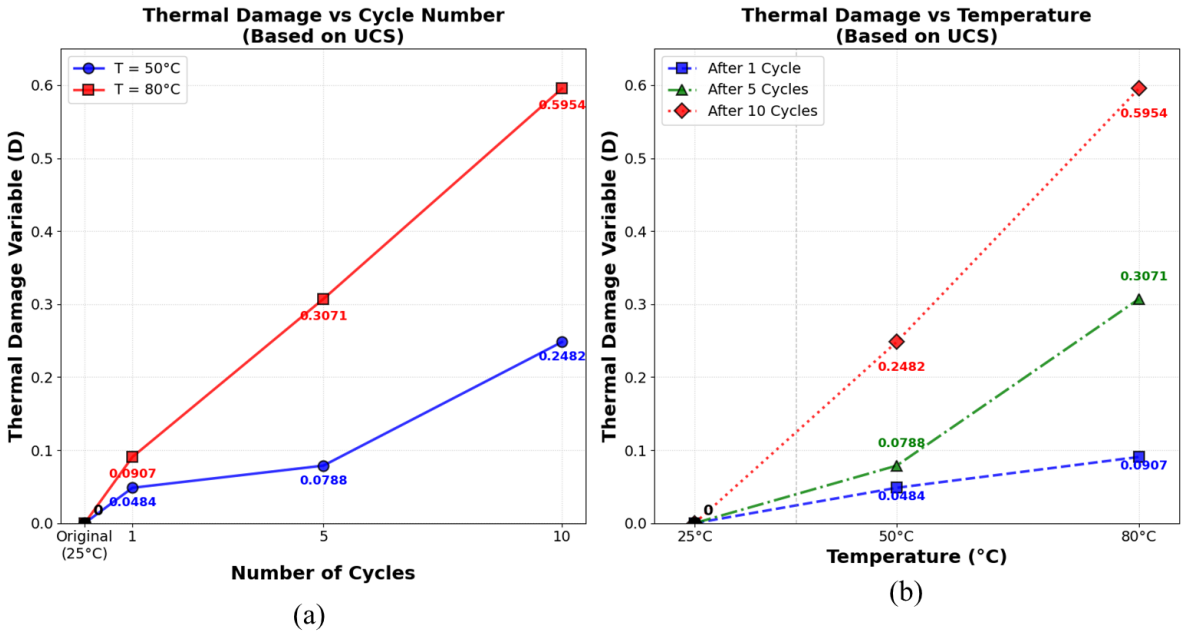


Fig. 10. Damage variable in the rock sample in terms of uniaxial compressive strength: (a) with increasing number of cycles (b) with increasing temperature

TABLE V. Damage variable values based on UCS and elastic modulus

| T (°C) | Cycle | D (UCS) | D (E) | D(E) sign |
|---|---|---|---|---|
| 25 | 0 | 0 | 0 | — |
| 50 | 1 | +0.05 | +0.11 | Damaged |
| 50 | 5 | +0.08 | −0.23 | Healed |
| 50 | 10 | +0.25 | +0.39 | Damaged |
| 80 | 1 | +0.09 | −0.64 | Strongly healed |
| 80 | 5 | +0.31 | −0.03 | Marginally healed |
| 80 | 10 | +0.60 | +0.81 | Severely damaged |

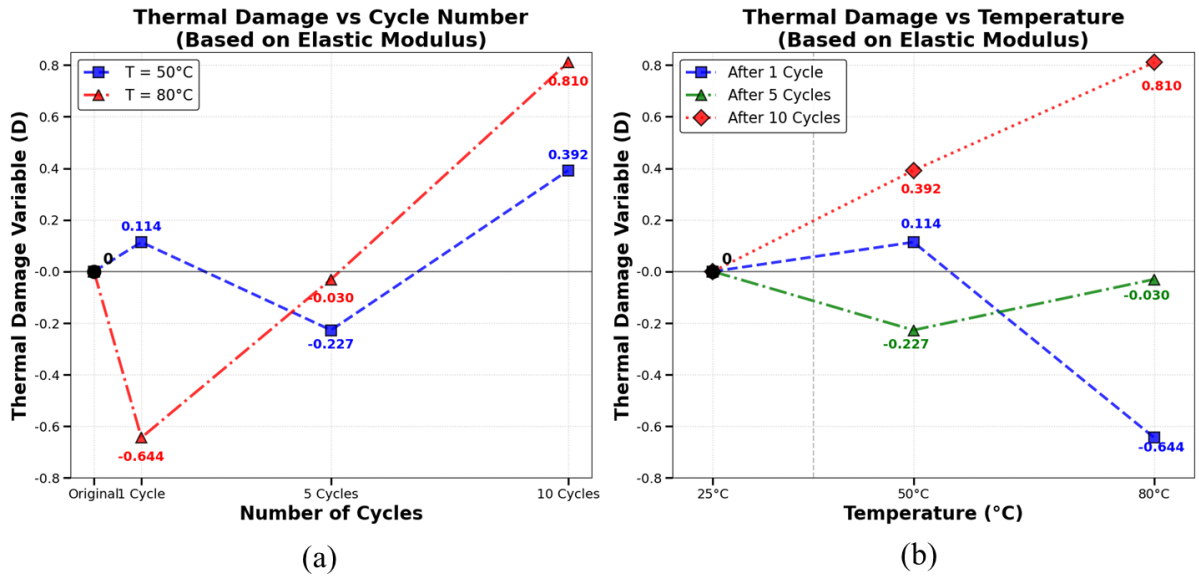


Fig. 11. Damage variable in the rock sample in terms of elastic modulus: (a) with increasing number of cycles, (b) with increasing temperature

The crack closure zone width is a direct indicator of how much pre-existing microcrack damage existed in the specimen before the test began. In the control specimen, this zone is narrow and low-stress, confirming that the intact material has very few open microcracks. The progressive widening of the crack closure zone with increasing temperature and cycle number reflects the accumulation of open microcracks induced by repeated thermal expansion and contraction. The particularly revealing case is 80°C after 10 cycles, where the material has so many open microcracks that it requires enormous deformation just to close them, yet they close so easily (closure stress of just 1.78 MPa) that the structural fabric has been almost completely compromised before any real load-bearing even begins.

The absence of Point B at all three 50°C conditions is physically meaningful. At 50°C, once the material enters its elastic phase, it behaves relatively coherently up to failure, microcracks do not begin propagating stably before peak load is reached. It is acknowledged that threshold identification from axial stress-strain data alone carries inherent uncertainty for ductile geomaterials such as rock salt, and future work incorporating lateral strain measurements or acoustic emission monitoring would provide more objective threshold detection.

At 80°C, the appearance of a distinct CD threshold in every specimen indicates a qualitatively different failure mechanism. The material begins accumulating unstable crack growth well before reaching its peak stress, creating a visible post-elastic but pre-peak nonlinear zone. The consistent B/C stress ratio of roughly 66–80% across all specimens that show Point B suggests this is a material-intrinsic proportion, maintained even as the absolute stress levels collapse.

The plastic zone widening by 115% from C=1 to C=10 at 80°C confirms that heavily cycled specimens sustain prolonged active cracking before finally failing, the hallmark of ductile damage accumulation replacing brittle fracture. The dramatic shrinkage of the elastic stress range at 80°C means the specimens have lost most of their capacity to store elastic strain energy, which directly explains both their reduced stiffness and their transition toward ductile behavior. The temperature effect on UCS is highly cycle-dependent. At C=1, the difference between 50°C and 80°C is only 1.17 MPa (4.4%), practically negligible. But at C=5, that gap widens to 6.32 MPa (33.0%), and at C=10 it reaches 9.61 MPa (85.8%). This non-linear interaction reveals that temperature and cycle number are not independent factors, they amplify each other synergistically, with high temperature making each additional cycle far more destructive than it would be at lower temperature.

The thermal stiffening at 80°C after C=1 is a physically real phenomenon in geomaterials. A single high-temperature cycle can cause thermal closure of pre-existing microcracks through mineral expansion, recrystallization of grain boundary cements, or partial sintering effects, temporarily producing a denser, stiffer microstructure than the original. The material essentially becomes over-consolidated by heat before damage accumulation begins to dominate at higher cycle counts. At 50°C, the mid-cycle stiffening suggests that at the relatively moderate temperature of 50°C, the material undergoes a two-phase response: initial mild loosening of grain contacts at C=1, followed by progressive crack healing, pore collapse, or thermal densification by C=5 that more than compensates.

Comparing the peak strength results with the elastic modulus analysis reveals an important contrast.

While elastic modulus showed a counterintuitive stiffening at early cycles (particularly the 2.17 GPa peak at 80°C, C=1), peak strength shows no such recovery, it decreases monotonically from the control at every step for both temperatures. This divergence indicates that thermal cycling can temporarily close and heal microcracks enough to restore or even enhance stiffness (since modulus is sensitive to crack aperture), but cannot restore the cohesive bonding and frictional interlocking between grains that ultimately determines how much stress the material can sustain before fracturing. Stiffness and strength are thus decoupled under thermal cycling, a material can become temporarily stiffer while simultaneously becoming permanently weaker, a distinction with significant implications for any structural or geotechnical application.

For 80°C, the modulus drops below the control value somewhere around C=6–8 based on the trajectory. For 50°C, C=1 is already below the control (1.17 GPa), C=5 rises above it (1.62 GPa), and C=10 falls well below (0.803 GPa). Both series ultimately end below the control, but via very different paths — one through a dramatic spike-and-crash, the other through a gentler dip-recovery-collapse pattern.

The 50°C series traces an unusual non-monotonic path through damage space that is best understood as three distinct phases. In the first phase, after one cycle at 50°C, D rises modestly to +0.11. This positive damage value confirms that a single moderate-temperature cycle does introduce genuine microstructural degradation — grain boundary microcracks open, some cementing bonds break, and the elastic modulus falls slightly below the intact value. In the second phase, between C=1 and C=5 at 50°C, the damage variable reverses sign entirely, dropping from +0.11 to −0.23. The physical explanation is thermal healing: repeated moderate heating causes progressive closure of pre-existing microcracks through mineral thermal expansion, recrystallization of grain contacts, and possible pressure solution or sintering at crack tips. By 5 cycles, these healing processes have accumulated enough to more than offset the cracking damage introduced simultaneously, producing a net stiffening effect that dominates. In the third phase, from C=5 to C=10 at 50°C, the healing mechanism is finally overwhelmed by cumulative fatigue damage, and D surges from −0.23 to +0.39.

The two observations of extended crack closure zone and increased elastic modulus at T=50°C between C=1 and C=5 are not contradictory because they measure different subsets of the crack population. Elastic modulus is controlled by a small number of structurally critical cracks that directly interrupt the load-bearing grain framework, specifically those oriented perpendicular to the loading direction. Thermal healing at 50°C preferentially closes these high-impact cracks through recrystallization and mineral expansion, restoring and even exceeding the original stiffness. The crack closure zone reflects the total open crack volume of all orientations and sizes, including mechanically non-critical cracks that contribute nothing meaningful to modulus but still require deformation to close under early loading. While the critical cracks are healing, repeated thermal cycling simultaneously generates new secondary cracks at grain boundaries and inclusion interfaces in non-critical orientations. These new cracks are invisible to the modulus but widen the closure zone.

After just one cycle at 80°C, D plunges to −0.64. At 80°C, the thermal expansion of mineral grains is substantially larger than at 50°C, generating far greater compressive stresses within the microstructure during the heating phase. These stresses forcibly close pre-existing microcracks, compact grain boundaries, and may induce partial sintering or thermally activated cementation at contact points. The result after a single cycle is a dramatically over-consolidated microstructure that far exceeds its original stiffness. However, this extreme negative D state is inherently unstable. The same high temperatures that drove the stiffening also introduced concentrated thermal stress fields at crack tips and grain boundaries. When the specimen is cooled after each cycle, differential thermal contraction opens new microcracks and widens existing ones.

The strongly negative D values observed at low cycle counts are physically consistent with thermally induced crack closure through mineral grain expansion, grain boundary compaction, and possibly thermally activated recrystallization mechanisms that have been reported in rock salt and other crystalline geomaterials under thermal loading [15, 16]. However, it must be acknowledged that the present study does not include direct microstructural observations such as SEM imaging, thin section petrography, or µCT scanning that would confirm densification or crack closure at the grain scale. The interpretation therefore remains inferential, supported by the mechanical measurements and by analogy with published microstructural evidence in similar materials. Future work incorporating in-situ microstructural monitoring during thermal cycling would be needed to directly validate this mechanism in rock salt.

The entire dataset can be understood through the competition between two opposing processes operating simultaneously in the material during thermal cycling. The first is thermal densification and crack healing: at moderate temperatures and low cycle counts, heat causes mineral expansion that closes microcracks, increases grain contact area, and temporarily raises stiffness above the original value. This mechanism dominates at 80°C after C=1 and at 50°C between C=1 and C=5. The second is thermal fatigue and microcrack accumulation: repeated

heating and cooling generates cyclic thermal stresses at grain boundaries due to differential expansion of different minerals. Over multiple cycles, these stresses propagate and open new microcracks faster than healing can repair them. This mechanism dominates at high cycle counts, especially at 80°C where the thermal stresses per cycle are larger, leading to the catastrophic 0.251 GPa result at C=10.

The blue dashed line connecting D = 0 (control), D = +0.11 (50°C), and D = −0.64 (80°C) after one cycle traces one of the most physically counterintuitive trends in the dataset. As temperature increases from 25°C to 80°C, the damage variable decreases, meaning higher temperature after one cycle produces less damage or even strong negative damage. This completely inverts the intuitive expectation and highlights why the number of cycles is an absolutely essential context for interpreting temperature effects on material behavior. By contrast, the red dotted line connecting D = 0 (control), D = +0.39 (50°C), and D = +0.81 (80°C) after ten cycles has a steep positive slope — higher temperature now consistently produces greater damage, and the relationship is approximately linear across the temperature range tested.

TABLE VI. PHYSICAL AND MECHANICAL PROPERTIES OF THE CONTROL SPECIMEN

| *Property* | *Symbol* | *Mean* | *Standard Deviation* | *Unit* |
|---|---|---|---|---|
| ***Static properties*** | | | | |
| Width | b | 80 | **±2** | mm |
| Height | h | 80 | **±2** | mm |
| Length(depth) | l | 80 | **-±2** | mm |
| Cross-sectional area | A | 6400 | **±8** | $mm^2$ |
| Density | $\rho$ | 2.19 | **± 0.2** | $g/cm^3$ |
| Unconfined Compressive Strength | UCS | 27.68 | ± 0.65 | Mpa |
| Static Young's modulus | $E_{stat}$ | 1.32 | ± 0.06 | Gpa |
| Static poisson's ratio | $\upsilon_{stat}$ | 0.195 | ±0.002 | - |
| ***Dynamic properties*** | | | | |
| Compressional wave velocity | $V_p$ | 4191.6 | ±5.58 | $^m/_s$ |
| Shear wave velocity | $V_s$ | 2560.3 | ±3.36 | $^m/_s$ |
| Dynamic shear modulus | $G_{dyn}$ | 14.35 | ± 0.038 | Gpa |
| Dynamic poisson's ratio | $\upsilon_{dyn}$ | 0.202 | ±0.0025 | - |
| Dynamic Young's modulus | $E_{dyn}$ | 34.5 | ±0.156 | Gpa |
| Dynamic Bulk modulus | $K_{dyn}$ | 19.3 | ±0.153 | Gpa |

## V. CONCLUSION

This study systematically investigated the coupled effects of temperature (50°C and 80°C) and repeated heating–cooling cycles (1, 5, and 10) on the mechanical behavior and damage evolution of rock salt under uniaxial compression, benchmarked against an intact control group tested at 25°C. The findings demonstrate that thermal cycling induces a complex, non-linear degradation process governed by the competition between two antagonistic mechanisms: thermal healing and densification at low cycle counts, and cumulative fatigue-driven microcrack growth at high cycle counts. The uniaxial compressive strength (UCS) results confirm monotonic and progressive reduction across all thermal conditions relative to the control value of 27.68 MPa. At 50°C, strength loss is initially gradual (4.8% after C=1, 7.9% after C=5) but accelerates sharply to 24.8% after C=10, revealing a non-linear damage threshold between five and ten cycles. At 80°C, degradation is significantly more severe: 9.1% reduction after C=1, escalating to 59.5% (11.20 MPa) after C=10. Critically, temperature and cycle number interact synergistically; the strength gap between 50°C and 80°C widens from 1.17 MPa at C=1 to 9.61 MPa at C=10, confirming elevated temperature dramatically amplifies the destructive impact of each additional cycle. The elastic modulus exhibits a counterintuitive non-monotonic response, initial stiffening followed by collapse. At 80°C after C=1, the modulus surges to 2.170 GPa (64.4% above control), reflecting thermal crack closure and grain boundary compaction. At 50°C, modulus recovers to

1.620 GPa at C=5 (22.7% gain). Both series collapse at C=10: 0.803 GPa (−39.2%) at 50°C and 0.251 GPa (−81.0%) at 80°C. This decoupling between stiffness and strength, whereby material becomes stiffer while permanently weaker, represents a key finding with significant implications for long-term structural assessment of salt caverns, as modulus is sensitive to crack aperture while UCS depends on cohesive bonding that thermal cycling cannot restore. Analysis of stress-strain thresholds reveals that the crack closure zone expands substantially with increasing temperature and cycle number, from 0.08% strain in the control to 1.22% at 80°C after C=10, reflecting progressive accumulation of open microcracks. Critically, the crack damage threshold is entirely absent in all 50°C specimens (indicating direct elastic-to-failure behavior) but appears distinctly in all 80°C specimens, signaling a qualitative shift to progressive crack propagation. The plastic zone widens by 115% from C=1 to C=10 at 80°C, quantitatively confirming progressive ductilization, while peak strain at 80°C accelerates with cycling, opposite to the saturating behavior at 50°C, indicating no upper limit reached by ten cycles.

The thermal damage variable D provides a unified framework: D(UCS) remains strictly positive and increases monotonically, progressing from +0.048 to +0.079 to +0.248 at 50°C and from +0.091 to +0.307 to +0.595 at 80°C. D(E) transitions from strongly negative at low cycles (−0.644 at 80°C, C=1) to severely positive at high cycles (+0.810 at 80°C, C=10), with the 50°C series tracing a non-monotonic path: +0.11 (C=1) → −0.23 (C=5) → +0.39 (C=10), capturing three phases of initial damage, thermal healing, and fatigue dominance. The critical transition from healing-dominated to damage-dominated behavior occurs between five and ten cycles for both temperatures, defining a practical operational threshold beyond which damage accumulation becomes irreversible and self-accelerating. From a practical standpoint, the permissible operating temperature of 80°C produces dramatically accelerated damage when combined with repeated injection–withdrawal cycles that induce thermal cycling of the surrounding rock mass, suggesting that limiting thermal cycle amplitudes and managing cycle frequency are as critical as controlling absolute temperature levels. The non-linear damage threshold between five and ten cycles underscores the importance of periodic structural monitoring and cycle-aware damage models in cavern stability assessments. The decoupling of stiffness and strength implies that monitoring elastic modulus alone is insufficient for assessing structural integrity; comprehensive monitoring must track multiple mechanical parameters including UCS, modulus, and acoustic emission activity. The progressive ductilization at 80°C indicates heavily cycled salt may transition toward a creep-prone state that could compromise cavern dimensional stability. Future work should incorporate direct microstructural observations (SEM, μCT) to validate inferred mechanisms, extend the cycle range beyond ten to characterize long-term damage saturation, include acoustic emission monitoring for real-time microcrack tracking, examine confining stress and pore fluid chemistry effects under in-situ conditions, utilize lateral strain measurements for robust threshold detection, and investigate faster thermal transients representative of rapid pressure drawdown events. In conclusion, this study demonstrates that thermal cycling of rock salt induces a complex degradation process governed by competition between thermal healing and cumulative fatigue damage, with the critical transition occurring between five and ten cycles and elevated temperature dramatically amplifying damage, while the decoupling of stiffness and strength provides significant implications for structural health monitoring, establishing a quantitative foundation for cycle-aware damage models and operational guidelines that prioritize both temperature control and cycle frequency management in the design of underground gas storage facilities.

## REFERENCES


[1] Blanco-Martín, L., Rutqvist, J., Battistelli, A., & Birkholzer, J. T. (2018). Coupled processes modeling in rock salt and crushed salt including halite solubility constraints: Application to disposal of heat-generating nuclear waste. Transport in Porous Media, 124, 159–182.

[2] Merey, Ş. (2019). Prediction of pressure and temperature changes in the salt caverns of Tuz Golu underground natural gas storage site while withdrawing or injecting natural gas by numerical simulations. Arabian Journal of Geosciences, *205*. https://doi.org/10.1007/s12517-019-4405-1

[3] Guo, W.; Li, J.; Wang, T.; He, T.; Xie, D.; Liao, Y.; Liu, C. Experimental Study on the Evolution Law of Permeability Characteristics of Salt Rocks Under Different Temperatures and Different Pore Pressures. Rock Mech. Rock Eng. 2025, 58, 1–23.

[4] Cemiloglu, A., Licai, Z., Arslan, S., Xu, J., Yuan, X., Azarafza, M., & Derakhshani, R. (2023). Support Vector Machine (SVM) Application for Uniaxial Compression Strength (UCS) Prediction: A Case Study for Maragheh Limestone. *Applied Sciences*, *13*(4), 1-14. Article 2217. https://doi.org/10.3390/app13042217

[5] Shi, J., Liu, G., Huang, P., & Ng, C. W. W. (2015). Interaction between a large-scale triangular excavation and adjacent structures in Shanghai soft clay. Tunnelling and Underground Space Technology, *50*, 282–295. https://doi.org/10.1016/j.tust.2015.07.013

[6] Aladejare, A. E. (2020). Evaluation of empirical estimation of uniaxial compressive strength of rock using measurements from index and physical tests. Journal of Rock Mechanics and Geotechnical Engineering, *12*(2), 256–268. https://doi.org/10.1016/j.jrmge.2019.08.001

[7] Askaripour, M., Saeidi, A., Rouleau, A., & Mercier-Langevin, P. (2022). Rockburst in underground excavations: A review of mechanism, classification, and prediction methods. Underground Space, *7*. https://doi.org/10.1016/j.undsp.2021.11.008

[8] Griffiths, L., Lengliné, O., Heap, M. J., Baud, P., & Schmittbuhl, J. (2018). Thermal cracking in Westerly Granite monitored using direct wave velocity, coda wave

interferometry, and acoustic emissions. Journal of Geophysical Research: Solid Earth, 123, 2246–2261. https://doi.org/10.1002/2017JB015191

[9] Barton, N. (2006). Rock quality, seismic velocity, attenuation and anisotropy.

[10] Bieniawski, Z. T. (1989). Engineering rock mass classifications: A complete manual for engineers and geologists in mining, civil, and petroleum engineering. John Wiley & Sons. ISBN: 978-0471601722

[11] Barton, N., Lien, R., & Lunde, J. (1974). Engineering classification of rock masses for the design of tunnel support. Rock Mechanics, 6(4), 189–236. https://doi.org/10.1007/BF01239496

[12] Hajizadeh,A and Taheri,E . (2025). Modeling the Behavior of Frozen Soil Under Freeze/Thaw Cycles with Emphasis on Depth and Temperature Change Rate Parameters. JOURNAL OF ROCK MECHANICS, 9(2), 29-41.

[13] Zhou, L., Zhu, Z., Oterkus, E., Oterkus, S., & Xu, H. (2023). Research on the effects of heating and cooling processes on the mechanical properties of yellow rust granite. Geohazard Mechanics, 1(3), 231–243. https://doi.org/10.1016/j.ghm.2023.09.001

[14] Brotóns, V., Tomás, R., Ivorra, S., & Alarcón, J. C. (2013). Temperature influence on the physical and mechanical properties of a porous rock: San Julián's calcarenite. Engineering Geology, 167, 117–127.

[15] Gautam, P. K., Dwivedi, R., & Kumar, A. (2021). Damage characteristics of Jalore granitic rocks after thermal cycling effect for nuclear waste repository. Rock Mechanics and Rock Engineering, *54*, 235–254. https://doi.org/10.1007/s00603-020-02260-7

[16] Isaka, A., Ranjith, P. G., Rathnaweera, T., Perera, M., Chandrasekharam, D., & Wanniarachchige, P. (2018). An influence of thermally-induced micro-cracking under cooling treatments: Mechanical characteristics of Australian granite. Energies, *11*(6), Article 1338. https://doi.org/10.3390/en11061338

[17] Guo, Y., Qin, Y., Xu, N., Lei, H., Xu, J., Zhang, B., Feng, S., & Chen, L. (2025). The influence of periodic temperature on salt rock acoustic emission, strength, and deformation characteristics. Applied Sciences, 15(16), Article 8848. https://doi.org/10.3390/app15168848

[18] Li, W., Zhu, C., Yang, C., Duan, K., & Hu, W. (2018). Experimental and DEM investigations of temperature effect on pure and interbedded rock salt. Journal of Natural Gas Science and Engineering, 56, 29–41. https://doi.org/10.1016/j.jngse.2018.05.020

[19] Liu, X., Wang, J., Wang, X., Lin, Y., Liu, X., & Song, Z. (2026). Fatigue properties and damage evolution of salt s rock after thermal cycling treatment. Rock Mechanics and Rock Engineering, 59(3). https://doi.org/10.1007/s00603-025-05026-1

[20] Li, W., Nan, X., Chen, J., & Yang, C. (2021). Investigation of thermal-mechanical effects on salt cavern during cycling loading. Energy, 232(9), 120969. https://doi.org/10.1016/j.energy.2021.120969

[21] ASTM D7012-23, "Standard test methods for compressive strength and elastic moduli of intact rock core specimens under varying states of stress and temperatures," ASTM International, West Conshohocken, PA, USA, 2023, doi: 10.1520/D7012-23.

[22] Maadikhah, A., Molladavoodi, H., Mortazavi, A., & Atapour, H. (2023). Experimental study of true triaxial loading effect on ultrasonic properties of rock salt. Rock Mechanics and Rock Engineering, *56*, 1–18. https://doi.org/10.1007/s00603-023-03436-7

[23] Davarpanah, S. M., Ván, P., & Vasarhelyi, B. (2020). Investigation of the relationship between dynamic and static deformation moduli of rocks. Geomechanics and Geophysics for Geo-Energy and Geo-Resources, *6*. https://doi.org/10.1007/s40948-020-00155-z

[24] Christaras, B., Auger, F., & Mosse, E. (1994). Determination of the moduli of elasticity of rocks. Comparison of the ultrasonic velocity and mechanical resonance frequency methods with direct static methods. Materials and Structures, *27*, 222–228. https://doi.org/10.1007/BF02473036

[25] Zhao, X. G., & Cai, M. (2010). A mobilized dilation angle model for rocks. International Journal of Rock Mechanics and Mining Sciences, 47(3), 368–384. https://doi.org/10.1016/j.ijrmms.2009.12.007

[26] Martin-Clave, C., Ougier-Simonin, A., & Vandeginste, V. (2021). Impact of second phase content on rock salt rheological behavior under cyclic mechanical conditions. Rock Mechanics and Rock Engineering, *54*(10), 5245–5267. https://doi.org/10.1007/s00603-021-02449-4

[27] Zhao, Y., Yang, Z., Wang, C., & Bi, J. (2023). Experimental study on damage self-healing and strain hardening of salt rock under secondary loading. *Rock and Soil Mechanics*, *44*(5),1457–1466. https://doi.org/10.16285/j.rsm.2022.0863

[28] Li, H., Dong, Z., Ouyang, Z., Liu, B., Yuan, W., & Yin, H. (2019). Experimental Investigation on the Deformability, Ultrasonic Wave Propagation, and Acoustic Emission of Rock Salt Under Triaxial Compression. *Applied Sciences*, *9*(4), 635. https://doi.org/10.3390/app9040635

نشریه‌ی مکانیک سنگ
JOURNAL OF ROCK MECHANICS
دوره نهم، شماره۴، زمستان ۱۴۰۴، صفحه ۷۳ تا ۹۱
https://doi.org/10.22034/IRSRM.2026.739361.1083

# ارزیابی اثر دما و تعداد چرخه گرم‌شدن-سردشدن برخرابی سنگ نمک

**علی کلانتری دهقی[۱]؛ ابراهیم فرخ[۱*]؛ حامد ملاداودی[۱]**
۱- دانشکده مهندسی معدن، دانشگاه صنعتی امیرکبیر، تهران، ایران.

**دریافت : ۱۴۰۴/۱۱/۰۲؛ پذیرش: ۱۴۰۴/۱۲/۲۹**
**(*نویسنده مسئول: e.farrokh@aut.ac.ir)**

**چکیده**

سنگ نمک به دلیل ویژگی‌هایی نظیر نفوذپذیری بسیار پایین، تخلخل اندک، رفتار ویسکوپلاستیک، قابلیت خودترمیمی و پایداری مناسب، به‌عنوان یکی از مهم‌ترین سنگ‌های میزبان در ذخیره‌سازی زیرزمینی گاز طبیعی، هیدروژن و همچنین دفن پسماندهای هسته‌ای شناخته می‌شود. بااین‌حال، در طی بهره‌برداری از مخازن نمکی، فرآیندهای تزریق و برداشت مکرر سیالات سبب ایجاد تغییرات دمایی متناوب و چرخه‌های حرارتی در توده سنگ می‌شوند. این چرخه‌ها با ایجاد انبساط و انقباض حرارتی مکرر، تنش‌های داخلی، رشد ریزترک‌ها و تغییرات ساختاری در سنگ نمک، می‌توانند خواص مکانیکی و فیزیکی سنگ را تحت تأثیر قرار داده و در بلندمدت موجب کاهش پایداری و ایمنی مخازن زیرزمینی شوند. ازاین‌رو، شناخت رفتار سنگ نمک تحت شرایط حرارتی مختلف از اهمیت ویژه‌ای برخوردار است. هدف اصلی این پژوهش بررسی تأثیر همزمان دما و چرخه‌های گرم‌شدن و سردشدن بر رفتار مکانیکی و میزان آسیب ایجادشده در سنگ نمک است. برای دستیابی به این هدف، نمونه‌های سنگ نمک با هندسه مکعبی تهیه شده و تحت سه سطح دمایی شامل دمای محیط (۲۵ درجه سانتی‌گراد)، ۵۰ و ۸۰ درجه سانتی‌گراد و همچنین در چرخه‌های حرارتی ۱، ۵ و ۱۰ قرار گرفتند. نتایج مطالعات نشان داد که افزایش دما و تعداد چرخه‌های حرارتی موجب تغییر محسوس در ساختار داخلی سنگ نمک و کاهش خواص مکانیکی آن مانند مقاومت فشاری تک‌محوره و مدول الاستیک می‌شود.

**واژگان کلیدی** **سنگ نمک، چرخه‌های حرارتی، دما، مقاومت فشاری تک‌محوره، آسیب**